Light-dependent ionic-electronic conduction in an amorphous octahedral molybdenum cluster thin film

Kenshi Harada, Thi Kim Ngan Nguyen, Fabien Grasset, Clothilde Comby-Zerbino, Luke Macaleese, Fabien Chirot, Philippe Dugourd, Noée Dumait, Stéphane Cordier, Naoki Ohashi, et al.

Harada et al. *NPG Asia Materials* (2022)14:21
https://doi.org/10.1038/s41427-022-00366-8

NPG Asia Materials

ARTICLE Open Access

Light-dependent ionic-electronic conduction in an amorphous octahedral molybdenum cluster thin film

Kenshi Harada[1], Thi Kim Ngan Nguyen[2,3], Fabien Grasset[3,4], Clothilde Comby-Zerbino[5], Luke MacAleese[5], Fabien Chirot[6], Philippe Dugourd[5], Noée Dumait[7], Stéphane Cordier[7], Naoki Ohashi[3,4], Motohide Matsuda[1] and Tetsuo Uchikoshi[3,4]

Abstract

We developed a new environment-sensing device based on the opto-ionic-electronic phenomena of an octahedral molybdenum metal (Mo_6) cluster. When the Mo_6 cluster is electrochemically deposited on a transparent electrode in an organic solvent containing a trace amount of water, the water permeates the deposited film. During the process, some ligand species that stabilize the frame structure of the Mo_6 cluster are substituted with hydroxyl groups, and the negatively charged frame structure of the Mo_6 cluster unit is stabilized by hydronium counterions. As a result, the transparent film of the Mo_6 cluster fabricated by this method exhibits ionic-electronic mixed conduction of the hydronium ion. The ionic conduction greatly changes depending on the temperature and humidity in the atmosphere, and the electrical conductivity greatly changes depending on the wavelength and intensity of the irradiated light. These unique multisensing properties present new possibilities for environmental sensing applications.

Introduction

Functional materials based on metals, semiconductors, ceramics, polymers, composites, etc. have provided solutions for societal problems and have led to the development of new technologies for industries[1]. In particular, materials that convert energy, such as thermal, chemical, optical, mechanical, or electrical energy, to one form or another are widely used in everyday situations. Nevertheless, more advanced material properties are required for devices such as piezoelectrics[2], thermoelectrics[3], gas sensors[4], and photodiodes[5] to realize a sustainable and safe society. In recent years, the miniaturization of equipment has resulted in innovative technological advances in various fields[6]. The development of multifunctional materials that can simultaneously detect different types of information using a single material will further expand the applications in sensing, miniaturization, and lightning devices. The effect of light on the electronic properties of ionic conductors near room temperature is a new and impressive topic that was recently discussed on a report on halide perovskites[7] and another on a polymeric ionic liquid[8]. We have focused on metal atom clusters, which are recognized as multifunctional building blocks of nanomaterials[9], with the aim of designing new smart devices (as a sensor for instance) that can utilize the optoelectronic and opto-ionic properties of such materials. Metal atom clusters, described as "a finite group of metal atoms which are held mainly together, or at least to a significant extent, by bonds directly between metal atoms, even though some nonmetal atoms may also be intimately associated with the cluster"[10] have a variety of interesting properties

Correspondence: Thi Kim Ngan Nguyen (NGUYEN.Thikimngan@nims.go.jp) or Motohide Matsuda (mm_2008@alpha.msre.kumamoto-u.ac.jp)
[1]Graduate School of Science and Technology, Kumamoto University, Kumamoto, Japan
[2]International Center for Young Scientists, ICYS-Sengen, Global Networking Division, National Institute for Materials Science, Tsukuba, Japan
Full list of author information is available at the end of the article

originating from their simple and unique structures and consisting of a limited number of elements. Among the metal clusters, molybdenum octahedral cluster compounds with the general formula $A_2Mo_6X^i_8L^a_6$ ($A = Cs^+$, n-$(C_4H_9)_4N^+$ and X = Cl, Br or I and L = Cl, Br, I, F, OH…, i = inner and a = apical) exhibit photochemical and redox properties due to the delocalization of the valence electrons on the metal centers[11]. The Mo_6 metallic core cluster is stabilized by eight face-capped inner ligands (Br^i) through Mo–Br^i bonds, which are dominantly covalent, and six additionally bonded apical ligands (Br^a) through the Mo–Br^a linkage, which has strong ionic character[12]. It is well known that these cluster compounds dissociate in solvents to form the $[Mo_6Br^i_8Br^a_6]^{2-}$ anionic units based on a rigid $\{Mo_6Br^i_8\}^{4+}$ block. In solution, the apical Br^a atoms on the cluster can be exchanged by functional groups. Previous studies of Mo_6 cluster-based materials revealed that they exhibit phosphorescence, photovoltaic photocatalytic activity, and photoconductivity under light irradiation[13,14]. The electrical conductivity of the Mo_6 cluster-based material was first described by a three-dimensional (3D) variable-range hopping mechanism based on the coronene radical cation[15]. A recent study suggested that compacted pellets of $[\{Mo_6X^i_8\}(OH)^a_4(H_2O)^a_2]\cdot 12H_2O$ prepared from $Cs_2[\{Mo_6Br^i_8\}Br^a_6]$ and $Cs_2[\{Mo_6Cl^i_8\}Cl^a_6]$ can conduct protons due the difference in resistance between wet and dry air at room temperature[16], although neither the origin of the carrier nor the conduction mechanism was clarified. Additionally, Nguyen et al. successfully developed a process for producing transparent homogeneous films based on Nb_6, Mo_6, and Ta_6 clusters using electrophoretic deposition (EPD)[17], which offers significant combinations of cost-effectiveness, long-range consistency in film thickness and surface morphology, size-scalability, high deposition rates, and site selectivity. The obtained cluster films exhibited high transmittance in the visible range and strong absorption in the UV and NIR ranges accompanied by a red luminescence emission originating from the Mo_6 clusters[18]. Nguyen et al. used X-ray diffraction (XRD), Fourier transformation infrared spectroscopy (FT-IR), X-ray fluorescence (XRF), and X-ray photoelectron spectroscopy (XPS) to reveal that the Mo_6 films formed by EPD had an amorphous structure, were missing all of the Cs^+ ions in the original cluster blocks, had H_3O^+ ions as alternate counter cations in place of the Cs^+ ions, exhibited OH^- in place of some apical Br^- ligands, and had few incorporated water molecules[19]. Therefore, proton conduction was expected for the Mo_6 cluster films formed by EPD; however, their electronic properties have never been evaluated.

In this study, we investigated the humidity and temperature dependence of the electronic properties of a translucent Mo_6 cluster film prepared by EPD. In addition, the conductivity under light irradiation was also studied. Based on the obtained results, the conduction mechanism of the membrane is discussed. Mass spectrometry was used to precisely determine the chemical composition of the Mo_6 cluster films prepared by EPD. In addition, the electronic properties of the film were evaluated in detail by AC impedance measurements and DC measurements, and the influence of light irradiation on the electronic and ionic properties was investigated.

Results

Morphology observation of the deposited film

The cross-sectional SEM image of the film deposited on an anodic substrate coated with an ITO layer by EPD is shown in Fig. 1a. The deposited film presented a homogeneous morphology and a relatively flat surface. Its thickness was approximately 1.6 μm.

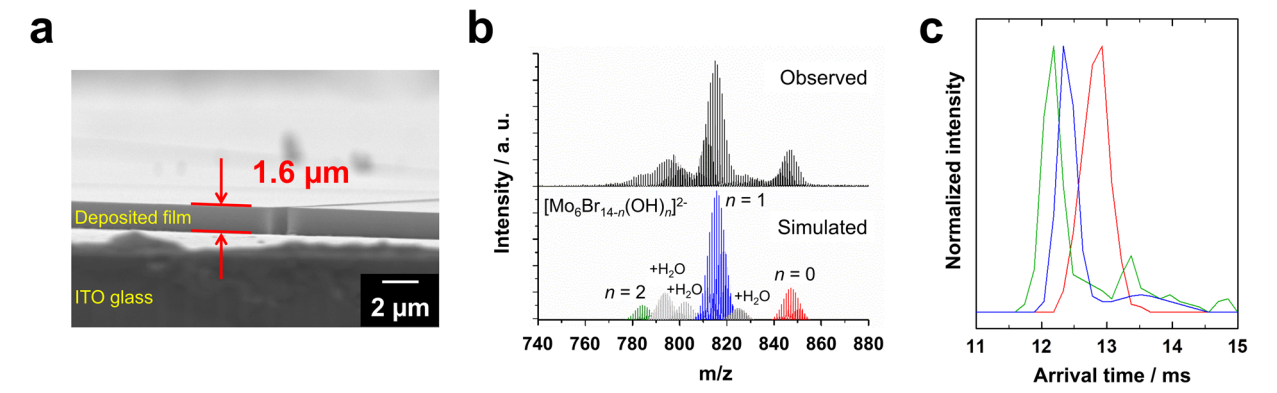

Fig. 1 Characterization of the cluster film fabricated by EPD. a Cross-sectional SEM image of the film deposited on an anodic substrate by EPD. **b** Observed and simulated electrospray ionization mass spectra for $[\{Mo_6Br^i_8\}Br^a_{6-n}(OH)^a_n]^{2-}$ ions with $n = 0$ (red line), 1 (blue line) and 2 (green line), and associated H_2O adducts (gray line). **c** ATDs recorded for the deposited film: $[\{Mo_6Br^i_8\}Br^a_{6-n}(OH)^a_n]^{2-}$; $n = 0$ (red line), $n = 1$ (blue line), $n = 2$ (green line). Drift conditions for the drift tube: 4.0 Torr helium at 298 K, drift voltage of 450 V.

Ion mobility spectrometry-mass spectrometry (IMS-MS)

The mass spectra dominated by the precursor in acetonitrile solution displayed a single isotope peak corresponding to $[\{Mo_6Br^i_8\}Br^a_6]^{2-}$ (see Supplementary Fig. 1a). The mass spectra resulting from the dissolution of the scraped films in acetonitrile were more complex. As emphasized in Fig. 1b, they were dominated by doubly charged anions, even though small amounts of the corresponding singly charged ions were also detected (see Supplementary Fig. 1b). In the following section, we focus on the dominant doubly charged species. From the isotope pattern simulations, the different spectral features were tentatively assigned to the ions with a general formula of the form $[\{Mo_6Br^i_8\}Br^a_{6-n}(OH)^a_n]^{2-}$, with n ranging from 0 to 2; other spectral features were attributed to water adducts of the latter ions. As shown in Fig. 1c, all the arrival time distributions (ATDs) of each species were dominated by a single peak, even though the signal-to-noise ratio was relatively low for the $[\{Mo_6Br^i_8\}Br^a_4(OH)^a_2]^{2-}$ anions. The width of the ATD peaks observed for the $[\{Mo_6Br^i_8\}Br^a_4(OH)^a_2]^{2-}$ and $[\{Mo_6Br^i_8\}Br^a_5(OH)^a]^{2-}$ anions is resolution-limited[20]; this phenomenon is consistent with the presence of single isomers or isomers with very similar structures, and the presence of a single isomer for those ions was indicative of CCS. In contrast, the $[\{Mo_6Br^i_8\}Br^a_6]^{2-}$ anions displayed a slightly broader peak. This may have resulted from the coexistence of different isomers with similar structures. However, it was difficult to isolate distinct populations by operating our instrument in tandem-IMS mode[21] and selecting only parts of the broad ATD peaks. This challenge could be due to coexisting species hidden under the broad ATD feature that undergo (<ms) fast interconversion in the gas phase[22]. The collision cross-sections (CCSs) were determined for the three observed complexes with 0, 1, and 2 substitutions and are listed in Supplementary Table 1. The experimental CCSs were very similar, displaying only a small contraction for each successive substitution (144 → 140 → 137 Å^2). The overall similarity was consistent with the absence of major structural rearrangement caused by the substitution. The small but distinguishable CCS contraction was consistent with the difference between the ionic radii of Br^- (196 pm) and OH^- (134 pm), as reported by Shannon et al.[23]. Interestingly, the CCS for the $[\{Mo_6Br^i_8\}Br^a_{6-n}(OH)^a_n]^{2-}$ species was similar to that of $[\{Mo_6Br^i_8\}Br^a_6]^{2-}$, which suggests that the overall structure of the cluster is conserved upon Br/OH exchange. The mass spectra clearly support our hypothesis that some of the apical Br^- ions are exchanged with OH during the EPD process[19], and IMS indicates that these ligand exchange reactions do not substantially affect the cluster geometry.

Temperature and humidity dependence of electric conductivity for Mo_6 cluster film

The impedance spectra of the cluster film measured at different temperatures under a fixed humidity of 80 RH% are shown in Fig. 2. It was found that the electronic resistance of the cluster film is temperature dependent; as the temperature increases, the semicircular arc decreases, corresponding to a decrease in the electronic resistance.

From the conductivity calculated from Fig. 2a, Arrhenius plots of the conductivity of the cluster film at humidities of 50 RH% and 80 RH% were created and are shown in Fig. 3a. The activation energies (E_a) were calculated from the Arrhenius plots, which were built on the dependence of conductivity on the temperature, represented by the following equation:

$$\sigma T = \mathrm{A}\exp(-E_a/RT) \quad (1)$$

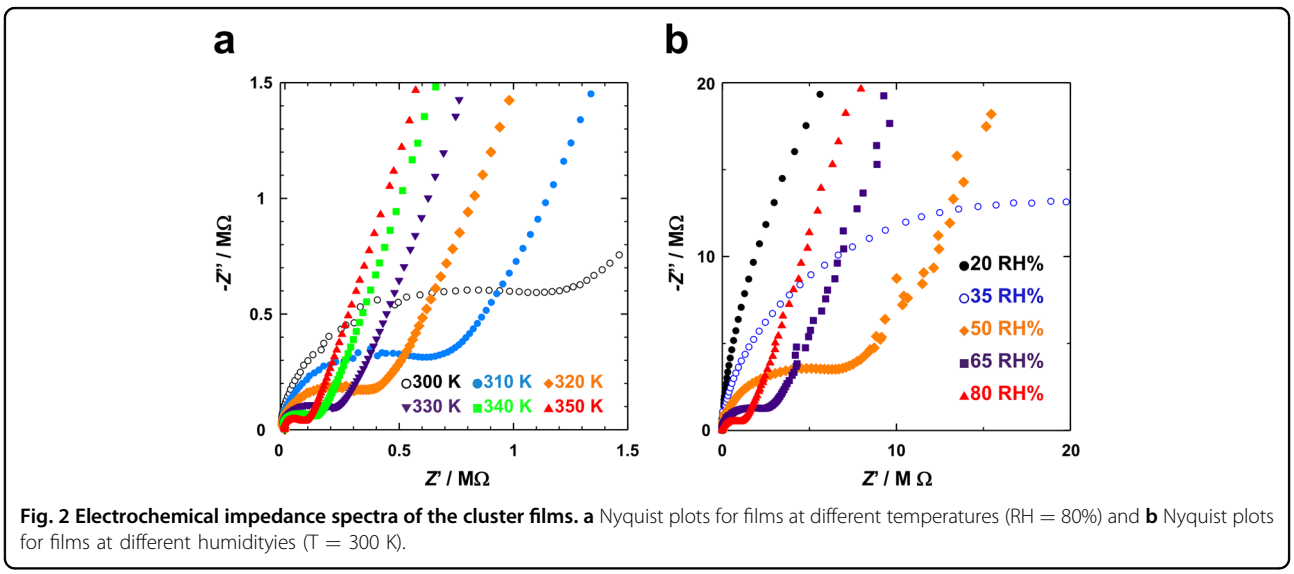

Fig. 2 Electrochemical impedance spectra of the cluster films. a Nyquist plots for films at different temperatures (RH = 80%) and **b** Nyquist plots for films at different humidityies (T = 300 K).

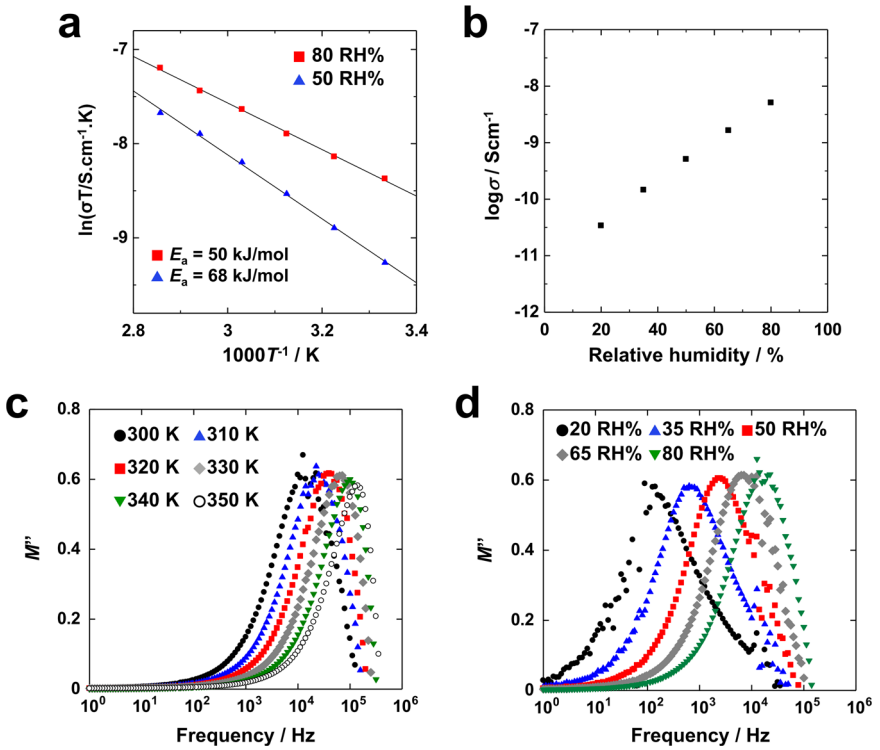

Fig. 3 Conduction properties of the amorphous octahedral molybdenum cluster thin film. a Temperature dependences of conductivity for the cluster film due to differences in humidity. **b** Humidity dependence of the conductivity at 300 K. **c** Frequency dependence of *M*″ at each temperature. **d** Frequency dependence of *M*″ at each humidity level.

where A is a constant, T is the temperature, R is the gas constant and E_a is the activation energy. The activation energies at relative humidities of 50 RH% and 80 RH% were estimated to be approximately 68 kJ/mol and 50 kJ/mol, respectively. Similar activation energies were obtained for the Mo_6 cluster films prepared with different deposition times, suggesting that the electronic properties are not affected by the film thickness of this sample size.

The impedance spectra of the cluster film measured at different relative humidities are shown in Fig. 2b. The temperature was fixed at 300 K for all the measurements. The electronic resistance of the cluster film was humidity dependence; as the relative humidity decreased, the semicircular arc became larger, indicating an increase in the electronic resistance. The relationship between the electric conductivity of the cluster film and the relative humidity at 300 K is shown in Fig. 3b. The film was prepared at a deposition time of 30 s. The conductivity of the sample prepared at a deposition time of 20 s is shown in Supplementary Fig. 2. The conductivity of the cluster films exponentially changed with increasing humidity, and the conductivities of the two samples prepared by EPD for 30 s and 20 s were similar.

Relaxation-frequency dependence of the Mo_6 cluster film by electric modulus analysis

The conductivity σ is given by

$$\sigma = ne\mu \tag{2}$$

where n is the carrier concentration, e is the charge of the carrier and μ is the mobility. The carrier in the cluster film was a cation introduced during the deposition process to compensate for the negative charge of the cluster unit. In general, the conductivity of the film depends on the number of H_3O^+ and OH^- ions created by the hydrolysis reaction during electrophoretic deposition (EPD). The local modification of pH around the electrodes is an important factor in the EPD process. The H_3O^+ ions were used to neutralize the Mo_6 cluster anions, and created clusters including $[Mo_6Br^i_8Br^a_4(H_2O)^a_2]$ and $[H_3O]_2[Mo_6Br^i_8Br^a_4(OH)^a_2]$ have been reported[19]. We assumed that the cluster film contained stable neutralized components. Moreover, it was recently demonstrated by Saito et al. that water molecules could be easily trapped in the chloride Mo_6 cluster compounds without causing changes to any apical ligands and that these molecules affect the optical properties[24]. For these reasons, the ligand exchange caused by water from humidity could

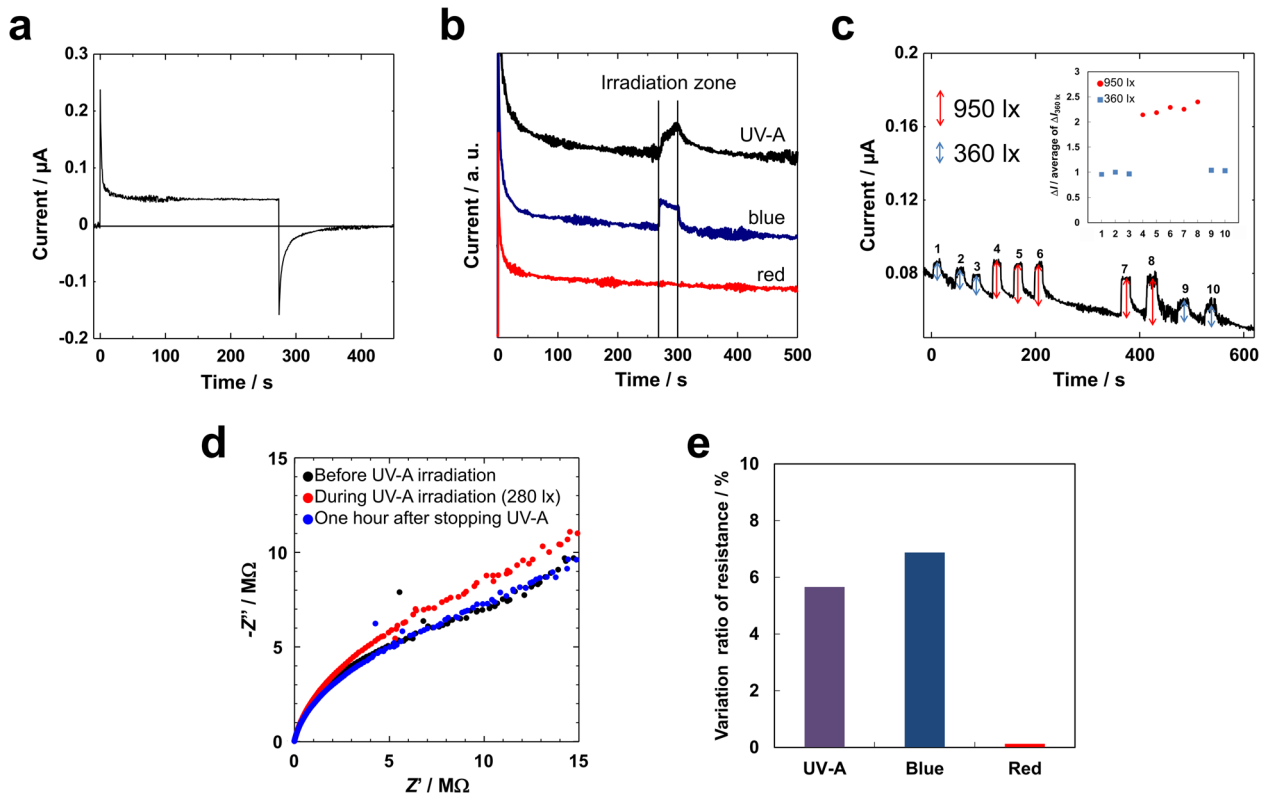

Fig. 4 Changes in the electronic properties of the cluster film due to light irradiation. a *I–t* curve with a 2 V applied DC voltage to the cluster film. **b** *I–t* curves of the cluster film under irradiation by UV-A, blue and red light. **c** Increase in current due to the different light strengths of UV-A. The inserted figure exhibits *ΔI*/average of $\Delta I_{360\ lx}$. **d** Impedance diagrams for the cluster film before, during, and after UV-A irradiation. **e** Change in resistance of the cluster film under UV-A, blue, and red light irradiation.

not occur. If this assumption is true, the carrier species and carrier density in the film remain unchanged. Thus, the temperature and humidity dependencies of the conductivity were likely caused by the different mobilities of the carrier.

In the present study, the electric modulus M^* was calculated by using the relation in Eq. (3), in which j is $\sqrt{-1}$, ω (= $2\pi f$) is the angular frequency, and C_0 is the geometric capacitance. M^* can be separated into real and imaginary parts; the imaginary Part M'' is given by Eq. (4), where f represents the frequency.

$$M^* = j\omega C_0 Z^* = M' + jM'' \tag{3}$$

$$M'' = 2\pi f C_0 Z' \tag{4}$$

The frequency dependence of the parameter M'' is shown in Fig. 3c, d. A plot of the relation between the value of M'' and the frequency is often used to evaluate ion conduction[25].

Figure 3c, d shows the frequency dependence of M'' at various **c** temperatures and **d** humidities. The frequency at the position of M''_{max} is known as the relaxation frequency. It shifts to a higher frequency with increasing temperature or humidity, indicating that the relaxation processes of the cluster film are affected by the temperature and humidity. The relationship between the f_{max} and relaxation time (τ) can be represented as $\tau = 1/2\pi f_{max}$; that is, τ decreases when the temperature and humidity increase. The temperature dependence of the relaxation time is shown in Supplementary Fig. 3. The temperature dependence of the relaxation time is expressed by the following equation:

$$\tau = \tau_0 \exp(-E_a/RT) \tag{5}$$

where τ_0 is a material-dependent preliminary factor. The estimated activation energy is approximately 48 kJ/mol, which is almost the same as the activation energy obtained from the Arrhenius plots of the conductivity. The relation between the conductivity and dielectric relaxation is expressed by the following equation:

$$\sigma = \varepsilon_0 \varepsilon_s / \tau \tag{6}$$

where ε_0 is the dielectric constant of the vacuum and ε_s is the static dielectric permittivity[26]. Notably, the conductivity increases when τ decreases in this equation.

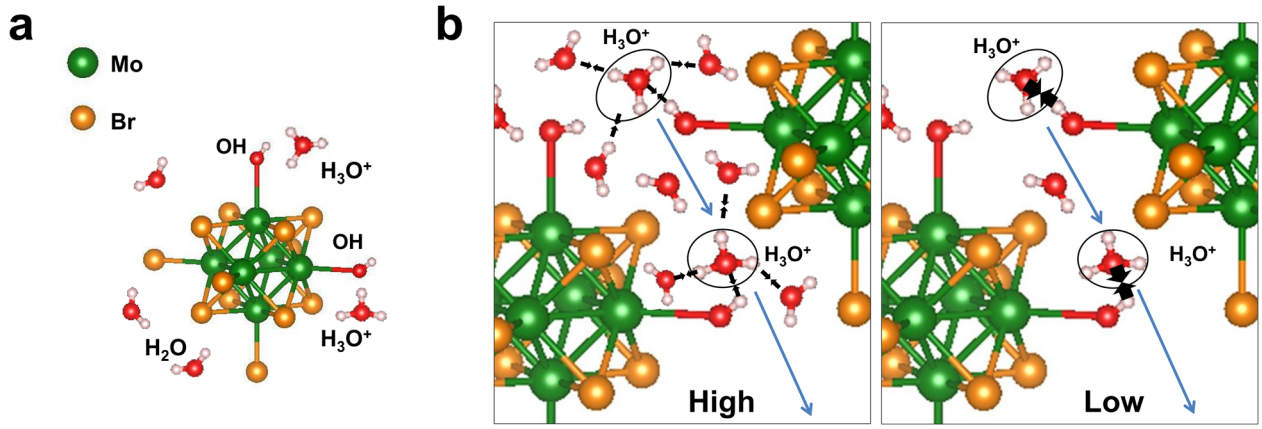

Fig. 5 Schematic illustration of the structure of the cluster film. a Octahedral molybdenum cluster in the film. **b** Structures postulated for the cluster films in high and low humidities.

Electronic properties of the Mo_6 cluster film under light irradiation characterized by DC measurement

The *I-t* curve obtained when a DC of 2 V was applied to the cluster film is shown in Fig. 4a. When the DC voltage was applied, the current immediately reached its maximum value and then decreased over time. Moreover, the current continued to flow slowly at a certain constant value after the current reduction almost stopped. When the current became constant, the application of the voltage was stopped. The flowing current was recorded as a negative value, and then it reached 0. Because ions are polarizable, the film is believed to act as an ion conductor[26]. In addition, a low current continued to flow after the abrupt reduction of the current at the initial stage when DC voltage was applied to the film, suggesting that it is due to electron conduction. In amorphous systems at low temperatures, transport is often dominated by hopping conduction. Electrical conduction in such a system is generally achieved through the incoherent transitions of the charge carriers between spatially localized states[27].

Figure 4b shows the *I–t* curve of the Mo_6 film under irradiation by UV-A, blue and red LED lights when DC was applied. In each case, light irradiation was performed for only 30 s after an elapsed time of 270 s from the start of the DC voltage application. When UV-A and blue light were used, a temporary increase in the current was observed; this increase was not observed when the sample was irradiated with red light. To clarify this behavior, an investigation into the abovementioned phenomenon by light irradiation was carried out by changing the illuminance of UV-A, as shown in Fig. 4c. As shown in Fig. 4c, when a strong light of 950 lx was applied, the current value was obviously increased by approximately 2.6 times that of current resulting form irradiation with weak light of 360 lx.

Electronic properties of the Mo_6 cluster film under light irradiation characterized by AC impedance measurements

Impedance measurements of the cluster film were performed under UV-A, blue and red light irradiation with illuminances of 280 lx, 100 klx, and 35 klx, respectively. The photon flux densities of these illuminances were roughly similar under the conditions. Figure 4d shows the impedance plots for UV-A LED light irradiation. The semicircular arc of the impedance was recorded to be slightly larger than that before irradiation, representing a decrease in the conductivity. Figure 4e shows the increasing rate of the impedance when the UV-A, blue, and red LED lights were irradiated. An increase in the impedance was clearly observed when the samples was irradiated with UV-A and blue light, while no significant changes were observed with red light, as expected.

Discussion

A schematic of the structure of the Mo_6 cluster in the film proposed from these results is shown in Fig. 5a. When the $Cs_2Mo_6Br_{14}$ powder is dispersed in methylethylketone (MEK), it dissociates into Cs^+ and $[\{Mo_6Br^i_8\}Br^a_6]^{2-}$ ions, and the two Br apical ligands at the maximum are simultaneously replaced with OH. The sites of the replaced Br apical ligands are random. Water molecules present in the MEK solvent generate H^+ by electrolysis on the electrode surface during the application of an electric field and then combine with H_2O to form H_3O^+. Thus, H_3O^+ ion acts as a counter cation to neutralize the negatively charged Mo_6 cluster unit deposited on the substrate. As a result, a new amorphous network is formed by the disordered arrangement of the modified Mo_6 clusters. In addition, the H_3O^+ counter cations coordinate with the substituted OH groups at the Br^a sites by hydrogen bonding, and many water molecules undergo similar hydrogen bonding interactions. Indeed, previous

experimental and simulation results clearly demonstrated the existence of HO − H* − OH bridges between adjacent cluster units, which seems to favor the vehicle diffusion model[16].

Based on the temperature- and humidity-dependent conductivity, it was clarified that the conduction mechanism is related to the water molecule content and mobility. According to the E_a of the Mo_6 cluster film, which is approximately 50–70 kJ/mol, the conduction mechanism of the cluster film is proposed to be the vehicle mechanism by which H_3O^+ moves[28]. Schematic illustrations of the proposed conduction mechanism are shown in Fig. 5b. Under high humidity conditions, more water molecules are incorporated into the film; they surround the hydronium ion coordinated to the apical OH ligands of the Mo_6 cluster, weaken the hydrogen bond, and allow the hydronium ion to easily move within the networks. As a result, the activation energy decreases at higher humidities. From the viewpoint of temperature, it is obvious that the conductivity increases with increasing temperature, corresponding to an increase in the mobility of the H_3O^+ ion.

As a result of the DC measurement, a large increase in the current due to light irradiation was confirmed. The measurement of the photoluminescence excitation (PLE) of the cluster film[14] revealed that the Mo_6 cluster is excited by light in the wavelength range of 370 and 470 nm, resulting in red light emission. These observations confirm that the electronic properties of the cluster film can be modified by UV-A and blue light irradiation. The Mo_6 cluster releases one electron when it is excited by light irradiation, and as a result, the Mo_6 cluster, which possesses 23 electrons, becomes a powerful oxidizing agent[29]. The excited electrons probably become free electrons and flow through the film when an electric field is applied.

As a result of the AC impedance measurement, the impedance increased by 6% and 7% when the sample was exposed to UV-A and blue irradiation, respectively. These highly reproducible phenomena are reversible, as observed in Fig. 4d for UV-A irradiation. The conductivity reduced by light irradiation was restored to the initial state after 1 hour of equilibration. Because the Mo_6 cluster exhibits photocatalytic properties, water molecules and/or hydronium ions contained in the film decompose in the photoreaction[13], resulting in decreased ionic conductivity. This mechanism is assumed to be possible due to the statistical distribution of ions located between the apical hydroxyl groups of adjacent clusters. Moreover, when carrier reduction occurs, the negative charge of the cluster unit decreases, and $Mo_6Br_{12}(H_2O)_2$ can form locally, as reported by Sleight et al.[30] The efficiency of the ionic conductivity of the Mo_6 cluster can be enhanced by the cluster complex containing an apical hydroxyl group with the formula $[\{Mo_6X^i_8\}L^a_{6-x-y}(OH)^a_x(H_2O)^a_y]^{y-2}$ (X = L = Cl, Br, I; $x + y \le 6$). In addition, the control of the intensity of the H_3O^+ ion created by hydrolysis during electrophoretic deposition also contributes to the increase in ionic conductivity. Similar clusters with Cl and I as inner ligands were also tested. Very recently, A. Renaud et al. demonstrated the ambipolar properties via the integration of $[\{Mo_6I_8\}I_4(H_2O)_2]\cdot xH_2O$ as light harvesters in an all-solid solar cell[31]. A significant photoresponse with a typical diode characteristic clearly provides evidence of the simultaneous transfer and transport of holes and electrons within the $[\{Mo_6I_8\}I_4(H_2O)_2]\cdot xH_2O$ layer. Such molecular structure-based layers naturally lead to intrinsic semiconducting behavior.

Based on these experiments, the dependence of the humidity, irradiated light strength, and irradiation wavelength on the electronic properties of the Mo_6 cluster film was demonstrated for the first time. Taking into account the most advantageous characteristics of the Mo_6 cluster, such as the large Stokes shift, long lifetime and high red luminescent efficiency, the EPD film is a promising multifunctional device for humidity and UV-light sensing.

Materials and methods

Preparation of cluster film by EPD

$Cs_2Mo_6Br_{14}$ powder was synthesized from $MoBr_2$ and CsBr by a solid-state method at high temperature[17]. The $Cs_2Mo_6Br_{14}$ powder was dissolved in reagent grade MEK (99.5%, Kishida Chemical Co., Ltd.) at a concentration of 5 g/L with agitation by a magnetic stirrer until a transparent solution was obtained[19]. ITO glass and a stainless steel sheet were connected to a DC power supply (PD56-10AD, KENWOOD) and served as the anodic substrate and cathode electrode, respectively. The ITO glass was washed with distilled water and ethanol by ultrasonication before use. EPD was carried out at a constant voltage of 15 V for 30 s. The Mo_6 cluster film deposited on the ITO glass substrate was characterized after drying in air for 24 h.

Mass spectrometry

IMS-MS measurements were performed using a home-made tandem drift tube combined with a quadrupole-time-of-flight mass spectrometer (Maxis Impact Bruker, Bremen, Germany) described elsewhere in detail[32,33]. To perform the IMS-MS measurements, the cluster film was first scraped from the ITO substrate, dissolved in 1 mL of acetonitrile, and then diluted in the same solvent to a final concentration of 50 µmol/L. For comparison, solutions of the precursor powder were prepared in acetonitrile at the same concentration. The solutions were directly injected into an electrospray source using a syringe pump (120 µL/h) and analyzed in negative ion mode. The electrospray ions were periodically injected into a 79-centimeter-long

drift tube filled with helium at a pressure of 4 Torr and maintained at 298 K. Drift voltages ranging from 250 to 500 V were applied across the tube to allow mobility separation. Mass-resolved ATDs were finally obtained by recording the mass spectra as a function of the arrival time of the ions at the end of the drift tube. Absolute CCSs were obtained without calibration by measuring the arrival times as a function of the inverse drift field based on the Mason-Schamp equation[20]. Following this procedure, the uncertainty of the absolute value of the CCS was estimated to be 2%.

AC impedance and DC measurement

The electrical conductivity of the cluster films was measured by the AC impedance method, which was carried out in the frequency range of 1–10^6 Hz under an applied voltage of 0.1 V using a potentio-galvanostat (IVIUMSTAT, Ivium Technologies). The electric circuit was assembled using a micrometer; the electrode was in contact with the cluster film at a constant force of 5.2 N. In addition, to maintain a constant test environment, the measurements were carried out in a thermo-hygrostat (SH-222, Espec Corp.) at fixed temperatures in the range of 300–350 K and a fixed relative humidity in the range of 20-80 RH% (Supplementary Fig. 4). The electrical conductivity was expressed by the following equation:

$$\sigma = l/(\mathrm{R.A}) \tag{7}$$

where σ is the electrical conductivity, l is the thickness of the film, A is the area of the sample (0.09 π cm^2), and R is the total resistance measured by electrochemical impedance spectroscopy (EIS). The Nyquist diagram was fitted by using a Randles equivalent circuit, as depicted in Supplementary Fig. 4.

Irradiation conditions

For the electrical conductivity measurement of the cluster film under UV-A or visible light irradiation, both the DC and AC impedance methods were applied. The AC impedance method was performed under the previously mentioned conditions. The DC measurements were performed under an applied voltage of 2 V (V_1) using a measurement system assembled as shown in Supplementary Fig. 4. LEDs with fixed wavelengths of 390–395 nm (UV-A), 465–475 nm (blue), and 660 nm (red) were used for light irradiation. In Supplementary Fig. 4, R1 is the shunt resistance, and V_2 is the voltage applied to the LEDs. The illuminance was measured using a luminometer (MT-912, URCERI). The measurements were carried out at 300 K and 50 RH%.

Acknowledgements
These studies were carried out as a part of the France-Japan International Collaboration Framework (UMI3629 LINK). The authors wish to thank Mr. D. Lechevalier of Saint-Gobain KK (Tokyo, Japan) and Dr. D. Berthebaud of CNRS for their significant support involved in LINK and related activities.

Author details
[1]Graduate School of Science and Technology, Kumamoto University, Kumamoto, Japan. [2]International Center for Young Scientists, ICYS-Sengen, Global Networking Division, National Institute for Materials Science, Tsukuba, Japan. [3]CNRS-Saint-Gobain-NIMS, IRL3629, Laboratory for Innovative Key Materials and Structures (LINK), International Collaboration Center, National Institute for Materials Science (NIMS), Tsukuba, Japan. [4]Research Center for Functional Materials, National Institute for Materials Science, Tsukuba, Japan. [5]Univ Lyon, Université Claude Bernard Lyon 1, CNRS, Institut Lumière Matière, Lyon, France. [6]Univ Lyon, CNRS, Université Claude Bernard Lyon 1, ENS de Lyon, Institut des Sciences Analytiques, UMR 5280, 5 rue de la Doua, Villeurbanne, France. [7]Univ. Rennes, CNRS, Institut des Sciences Chimiques de Rennes, Rennes, France

Author contributions
Kenshi Harada conceived and designed the experiments, performed the experiments, analyzed and interpreted the data, and drafted the article. Thi Kim Ngan Nguyen and Fabien Grasset conceived and designed the experiments; analyzed and interpreted the data; and drafted the article. Clothilde Comby-Zerbino, Luke MacAleese, Fabien Chirot and Philippe Dugourd analyzed and interpreted the data and drafted the article. Noee Dumait performed the experiments. Stephane Cordier and Naoki Ohashi revised critically for important intellectual content. Motohide Matsuda and Tetsuo Uchikoshi conceived and designed the experiments; analyzed and interpreted the data; and drafted the article.

Conflict of interest
The authors declare no conflicts of interest.

Supplementary information The online version contains supplementary material available at https://doi.org/10.1038/s41427-022-00366-8.

Received: 22 November 2021 Revised: 18 January 2022 Accepted: 24 January 2022
Published online: 11 March 2022

References

1. Lee, G. et al. Multifunctional materials for implantable and wearable photonic healthcare devices. *Nat. Rev. Mater.* **5**, 149 (2020).
2. Guerin, S., Tofail, S. A. M. & Thompson, D. Organic piezoelectric materials: milestones and potential. *NPG Asia Mater.* **11**, 10 (2019).
3. Dhawan, R. et al. $Si_{0.97}Ge_{0.03}$ microelectronic thermoelectric generators with high power and voltage densities. *Nat. Commun.* **11**, 4362 (2020).
4. Kumar, R., Zheng, W., Liu, X., Zhang, J. & Kumar, M. MoS_2-Based nanomaterials for room-temperature gas sensors. *Adv. Mater. Tech.* **5**, 1901062 (2020).
5. Mauthe, S. et al. High-speed III-V nanowire photodetector monolithically integrated on Si. *Nat. Commun.* **11**, 4565 (2020).
6. Liu, C. Recent developments in polymer MEMS. *Adv. Mater.* **19**, 3783–3790 (2007).
7. Kim, G. Y. et al. Large tunable photo effect on ion conduction in halide perovskites and implications for photodecomposition. *Nat. Mater.* **17**, 445–449 (2018).
8. Nie, H. et al. Light-controllable ionic conductivity in a polymeric ionic liquid. *Angew. Chem. Int. Ed.* **59**, 5123–5128 (2020).
9. Cordier, S. et al. Inorganic molybdenum octahedral nanoclusters, versatile functional building block for nanoarchitectonics. *J. Inorg. Organomet. Polym. Mater.* **25**, 189–204 (2015).

10. Cotton, F. A. Metal atom clusters in oxide systems. *Inorg. Chem.* **3**, 1217–1220 (1964).
11. Chakraborty, I. & Pradeep, T. Atomically precise clusters of noble metals: emerging link between atoms and nanoparticles. *Chem. Rev.* **117**, 8208–8271 (2017).
12. Perrin, A. & Perrin, C. Low-Dimensional Frameworks in Solid State Chemistry of Mo Cluster Chalcohalides. *Eur. J. Inorg. Chem.* **2011**, 3848–3856 (2011).
13. Ivanova, M. N. et al. Hexamolybdenum clusters supported on exfoliated h-bn nanosheets for photocatalytic water purification. *Inorg. Chem.* **59**, 6439–6448 (2020).
14. Nguyen, T. K. N. et al. Zn−Al layered double hydroxide film functionalized by a luminescent octahedral molybdenum cluster: ultraviolet−visible photoconductivity response. *ACS Appl. Mater. Interfaces* **12**, 40495–40509 (2020).
15. Yoshida, Y. et al. Isotropic three-dimensional molecular conductor based on the coronene radical cation. *Eur. J. Inorg. Chem.* **2014**, 3871–3878 (2014).
16. Daigre, G. et al. Metal atom clusters as building blocks for multifunctional proton-conducting materials: theoretical and experimental characterization. *Inorg. Chem.* **57**, 9814–9825 (2018).
17. Nguyen, T. K. N. et al. Extended study on electrophoretic deposition process of inorganic octahedral metal clusters: Advanced multifunctional transparent nanocomposite thin films. *Bull. Chem. Soc. Jpn.* **91**, 1763–1774 (2018).
18. Kirakci, K., Cordier, S. & Perrin, C. Synthesis and Characterization of $Cs_2Mo_6X_{14}$ (X = Br or I) Hexamolybdenum cluster halides: Efficient Mo_6 cluster precursors for solution chemistry syntheses. *Z. Anorg. Allg. Chem.* **631**, 411–416 (2005).
19. Nguyen, T. K. N. et al. Formation mechanism of transparent Mo_6 metal atom cluster film prepared by electrophoretic deposition. *J. Electrochem. Soc.* **164**, 412–418 (2017).
20. Revercomb, H. E. & Mason, E. A. Theory of plasma chromatography/gaseous electrophoresis. *Rev. Anal. Chem.* **47**, 970–983 (1975).
21. Trimpin, S. et al. Profiling of phospholipids and related lipid structures using multidimensional. *Int. J. Mass Spectrom.* **287**, 58–69 (2009).
22. Poyer, S. et al. Conformational dynamics in ion mobility data. *Anal. Chem.* **89**, 4230–4237 (2017).
23. Shannon, R. D. Revised effective ionic radii and systematic studies of interatomic distances in halides and chalcogenides. *Acta Crystallogr. Sect. A* **32**, 751–767 (1976).
24. Saito, N. et al. Solvent-mediated purification of hexamolybdenum cluster halide, $Cs_2[Mo_6Cl_{14}]$ for enhanced optical properties. *Cryst. Eng. Comm.* **19**, 6028–6038 (2017).
25. Badapanda, T., Harichandan, R. K., Nayak, S. S., Mishra, A. & Anwar, S. Frequency and temperature dependence behavior of impedance modulus and conductivity of $BaBi_4Ti_4O_{15}$ Aurivillius ceramic. *Process. Appl. Ceram.* **8**, 145–153 (2014).
26. Świergiel, J. & Jadżyn, J. Electric relaxational effects induced by ionic conductivity in dielectric materials. *Ind. Eng. Chem. Res.* **50**, 11935–11941 (2011).
27. Baranovskii, S. & Rubel, O. Charge transport in disordered materials. In: Kasap S., Capper P. (eds) Springer Handbook of Electronic and Photonic Materials. Springer Handbooks. Springer, Cham, (2017).
28. Shigematsu, A., Yamada, T. & Kitagawa, H. Wide control of proton conductivity in porous coordination polymers. *J. Am. Chem. Soc.* **133**, 2034–2036 (2011).
29. Nocera, D. G. & Gray, H. B. Electrochemical reduction of Molybdenum(II) and tungsten halide cluster ions. Electrogenerated chemiluminescence of $Mo_6Cl_{14}^{2-}$. *J. Am. Chem. Soc.* **106**, 824–825 (1984).
30. Guggenberger, L. J. & Sleight, A. W. Structural and bonding characterization of molybdenum dibromide, $Mo_6Br_{12}2H_2O$. *Inorg. Chem.* **8**, 1113 (1969).
31. Renaud, A. et al. Evidence of the ambipolar behavior of Mo_6 cluster iodides in all-inorganic solar cells: a new example of nanoarchitectonic concept. *ACS Appl. Mater. Interfaces* **14**, 1347–1354 (2021).
32. Simon, A. L. et al. Tandem ion mobility spectrometry coupled to laser excitation. *Rev. Sci. Instrum.* **86**, 094101 (2015). 10 pages.
33. Comby-Zerbino, C., Dagany, X., Chirot, F., Dugourd, P. & Antoine, R. The emergence of mass spectrometry for characterizing nanomaterials. Atomically precise nanoclusters and beyond. *Mater. Adv.* **2**, 4896–4913 (2021).